Model for Secondary Nucleation in a Suspension Crystallizer

Ruairi O. Meadhra, Herman J. M. Kramer, and Gerda M. Van Rosmalen
Laboratory for Process Equipment, Delft University of Technology, 2628 CA Delft, The Netherlands

A model that makes it possible to evaluate the secondary nucleation rate in a pilot-scale industrial crystallizer is presented. It relates the secondary nucleation rate directly to the volume rate of attrition of large parent crystals. Two other terms are included in the equality, one that expresses the distribution formed by the attrition fragments, and the other that expresses a survival efficiency accounting for the percentage of attrition fragments that grow out after the attrition step. The model is further tested on a 970-L draft-tube-baffled evaporative crystallizer with ammonium sulfate as the model material used for crystallization and having an on-line crystal size-distribution measuring device.

Introduction

The task of modeling secondary nucleation, has, in the past, been made difficult by the fact that very few experimental data were available over sustained periods of time with which quantitative relationships could be derived between the rate of secondary nucleation and the rate of attrition of the parent crystals.

Because of this, the rate of secondary nucleation was modeled as an "effective" nucleation rate and was related empirically to parameters describing the energy input to the crystallizer, the growth rate of crystals, and a parameter representing the crystal size distribution (CSD), such as the second or third moment of the distribution. These correlations do not perform accurately (see Results section), when modeling the dynamics of crystallizing systems, and also the fact that these correlations are empirical in nature, means that they give little insight into the mechanism of secondary nucleation. Moreover, they miss the vital link with the process of attrition from which the nuclei originate. Further, they also use the "effective" nucleation rate as a boundary condition depositing the total number of secondary nuclei at one point along the crystal length axis, ignoring the fact that a distribution of fragments is produced.

Much experimental work has been done in evaluating the rate of production of attrition fragments for several different materials under nongrowing conditions. To allow an accurate measurement of the attrition rate to be made, sharp crystal fractions were suspended in either saturated solutions or inert liquids and mixed using any one of a number of suspension impellers (Mazarotta, 1991; Jager, 1990). Using this method, a length dependent attrition function could be built, including parameters accounting for the effects of the impeller type and power input to the crystallizer. This approach assumes that the rate and source of attrition fragment production, as well as the distribution formed by the fragments under conditions of nongrowth, will satisfactorily reflect the same quantities under conditions of growth in a suspension crystallizer. This is highly unlikely as the crystals loose their sharp edges and corners under nongrowing conditions.

The main objective of this article is to show that it is possible to model secondary nucleation in a suspension crystallizer using only CSD data obtained from a continuous crystallization of ammonium sulfate. This is done by assuming a length-dependent attrition function and by directly relating the volume of attrited particles to the secondary nucleation rate via a survival factor. Two parameters are also incorporated to describe the position and spread of the attrition particle distribution. The model is a first attempt at defining a general procedure for the modeling of secondary nucleation in a crystallizer. The model is validated only for the case of ammonium sulfate crystallization in this contribution.

Theory of Secondary Nucleation Models

Empirical power law

The notion of modeling the CSD in a crystallizer using the model assumptions associated with the mixed-suspension–mixed-product-removal (MSMPR) concept has been used by

Correspondence concerning this article should be addressed to H. J. M. Kramer.

many workers to simulate the CSD present at steady state in a crystallizer (O'Dell and Rousseau, 1978; Rojkowski, 1993). This concept results in a straight-line function by plotting the logarithm of the population density function [$n(x)$ (#/m^4)] against the crystal size [x(m)]. The slope of this line is determined by the growth rate of the crystals (G_{kin}) and the residence time (τ) of the suspension in the crystallizer, according to the MSMPR equation

$$\ln[n(x)] = \ln(n_o) - \frac{x}{G_{\text{kin}}\tau}, \tag{1}$$

where n_o is the population density in the first size class formed by a secondary nucleation process. When comparing the function predicted by the MSMPR theory with the real distribution measured in a crystallizer at steady state, several deviations are apparent. In the large particle size ranges (Figure 1), a downward curvature is seen, which indicates that, assuming a well-mixed system, there is a reduction in growth rate at these sizes. This reduction in growth rate has been attributed to crystal attrition and has been modeled as a negative growth rate [$G_{\text{attr}}(x)$] (Jager et al., 1991). In the small particle-size ranges, an upward curvature is observed in the $\ln[n(x)]$ vs. x plot. This deviation has been attributed to the observation that in reality, crystals are born over a distribution of sizes and exhibit size-dependent growth (SDG) and growth rate dispersion (GRD) up to sizes of 80 to 100 μm, giving rise to this upward curvature (Rusli et al., 1980; Rojkowski, 1993). To account for these phenomena, accurate knowledge of such a birth function and also of the initial growth rates of secondary nuclei is required. As this information is in most instances not available, the problem is overcome by assuming that all particles grow at the same rate, and an "effective" nucleation rate is used [$B_{o,\text{eff}}$ (#/m^3·s)] whereby crystals are born at a size close to zero as in the MSMPR concept. Over the years, many correlations have been proposed for the effective rate of secondary nucleation, which are related to properties of the crystallizing solution, such as the supersaturation or growth rate [σ, $G_{\text{kin}}(\sigma)$], the mechanical agitation in the crystallizer (impeller speed or power input, N, ϵ), and a property representing the crystal-size distribution (CSD), such as the mass holdup (M_p),

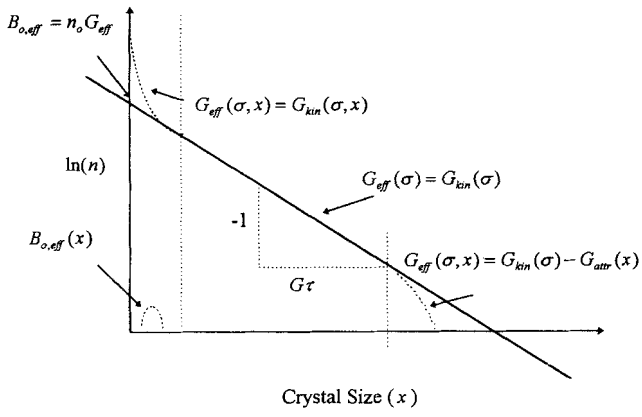

Figure 1. Plot of ln (population density) vs. crystal length, MSMPR, and deviations.

$$B_o \sim \sigma^b N^h M_p^j \sim G_{\text{kin}}^i \epsilon^k M_p^j. \tag{2}$$

Empirical in nature, these correlations give poor descriptions of the dynamics of the systems (see Results section) on which they are modeled. The power law has also been used as scale-up criteria, but judging from the volume of published data on the subject (see, for example, Grootscholten et al., 1982; Garside and Jancic, 1979; Bourne and Hungerbuehler, 1980), no rigorous method has yet been developed to use the equation to predict the secondary nucleation rate of different materials on different scales based on information regarding vessel geometry and properties of the materials. Also, being empirical, the power law gives little insight into the mechanism behind secondary nucleation.

Mechanistic models

In early descriptions of secondary nucleation, Ottens et al. (1972) and Botsaris (1976) proposed that the secondary nucleation rate could be related to three factors:

$$B_o = \dot{E}_t F_1 F_2, \tag{3}$$

where ($\dot{E}_t$) represents the rate of energy transfer to the crystal, F_1 is the number of attrition entities produced per unit of collision energy, and F_2 is the fraction of entities that survive to become nuclei.

Later, Mersmann et al. (1988) attempted to make a more precise estimate of the volume of material attrited from a parent crystal by introducing material parameters into the modeling procedure. To do this, the theory of Herz-Huber (Landau and Lifschitz, 1986) for the elastic interactions between two bodies was used, thus enabling the attrited volume to be calculated. Another notion introduced in this work was the idea of target efficiencies, whereby the probability of a collision between a crystal and the impeller could be calculated based on considerations of particle size and impeller geometry and rotational speed. By evaluating all these factors, the volume rate of attrition ($\dot{V}_{\text{attr}}$) could be calculated, which could then be related to the effective nucleation rate ($B_{o,\text{eff}}$), by the following expression:

$$B_{o,\text{eff}} \approx \frac{m_{a,\text{eff}}}{m_{a,\text{tot}}} \frac{\dot{V}_{\text{attr}}}{k_v x_{\text{attr}}^3}. \tag{4}$$

The second group of terms in Eq. 4 represents the number of all loose fragments produced by attrition ($\dot{E}_t F_1$), while the first represents the fraction of the total mass of produced particles that act as effective secondary nuclei (F_2).

In reality, then, this work also consists of a two-step process similar to those proposed by Ottens et al. (1972) and Botsaris (1976).

In 1990, Daudey et al. proposed a more detailed three-step model to describe secondary nucleation, which was consistent with experimental observations of the growth behavior of secondary nuclei and also attempted to account for the formation of surface growth structures of crystals in suspension. They defined two sources of nuclei, the first leading to the production of nuclei by attrition of macrosteps or other

growth *formations* (F) on the crystal surface, a mechanism that they termed *surface breeding*, and the second related to the attrition of portions of the crystal lattice, which could not previously have been identified as possible sources of nuclei. This manner of production they termed *mechanical breeding*, and would be the category into which previous modeling of secondary nucleation would fall. Further, they suggested that the surface-relief-related nuclei and the mechanical fragments would exhibit different (*survival* and *outgrowth* ($\eta_{\text{outgrowth}}$)) kinetics, as mechanical fragments may be more stressed than surface-relief fragments (Garside and Larson, 1978). In equation form, then, the effective nucleation rate is given by

$$B_{o,\text{eff}} = \eta_{\text{outgrowth}} \eta_{\text{removal}} F. \tag{5}$$

In this equation again, the last two terms ($\eta_{\text{removal}} F$) can be lumped together to express the total number of attrition particles released by the parent crystals, while the first term ($\eta_{\text{outgrowth}}$) expresses the fraction of these particles that grow out to larger sizes.

Working within the same framework, Van der Heijden et al. (1994), assuming a spiral growth mechanism, refined this theory by introducing parameters accounting for the height and the number density of steps on the crystal surface. They also pointed out that the amount of impurities present in the suspension are of great importance in determining the rate of production of secondary nuclei. The adsorption of such impurities would lead to weak points in the crystal lattice between successive layers of macrosteps, making them more susceptible to attrition processes. Also, the level and type of impurities in the suspension effects the number and height of steps on the crystal surface. Both of these effects support the notion of a surface breeding mechanism suggested by Daudey et al. (1990). It has already been shown that such growth entities are responsible for the formation of secondary nuclei (Van der Heijden and Elwenspoek, 1990). In a separate article (Van der Heijden et al., 1989), they showed that a distribution of fragments was produced by contacting a stationary crystal surface with a steel rod. The distribution of fragments took the form of a log-normal distribution with a median size of about 9 μm. Nienow and Conti (1978) detected distributions having a lower limit of 1 μm and a mean size of 5 μm in abrasion experiments using copper sulfate crystals. Other workers (Youngquist and Randolph, 1972) have shown that by suspending samples of crystals in a crystallizer, secondary nuclei in the size range < 3 μm were produced. A lower limit to the size of secondary nuclei produced could not be detected due to restrictions in the range of the CSD measuring instrument. Similar measurements for potash alum contact nuclei (Rusli et al., 1980) have shown similar results, where a large number of nuclei smaller in size than 4 μm were detected. These crystals were further shown to grow very slowly or not at all.

Assuming that attrition fragments are distributed over a range of sizes [$H(x)$], Eq. 5 becomes:

$$B_{o,\text{eff}}(x) = \eta_{\text{outgrowth}} \eta_{\text{removal}} H(x) F. \tag{6}$$

Note that the secondary nucleation rate is given in terms of number density (#/m^4·s), being a length-dependent function, unlike in the literature references given earlier, where it is given as the total number of attrition particles (#/m^3·s), and used as a boundary condition.

New Model

Keeping the framework described in the preceding section in mind, an example of how to determine the secondary nucleation rate is given below, for the specific case of ammonium sulfate crystallization for which much kinetic information regarding attrition is available.

Many correlations for the attrition rate [$G_{\text{attr}}(x)$] exist that are normally taken as functions of particle length only. It has been shown that the following expression satisfactorily describes the attrition rate in the draft tube crystallizer under study in this work (Eek et al., 1995) for ammonium sulfate crystallization:

$$G_{\text{attr}}(x) = K'_{\text{attr}}\left(1 - \left\{1/\left[1 + (x/x_g)^n\right]\right\}\right). \tag{7}$$

The length term x in this equation could also be expressed as the surface area ($\propto x^2$) or the volume of the crystal ($\propto x^3$), thus reducing the power in the attrition function appropriately.

The deviation in the MSMPR ln [$n(x)$] vs. x line due to attrition of large particles is shown in Figure 1.

The correlation in Eq. 7 contains three unknown parameters (K'_{attr}, x_g, n), which must be evaluated from experimental CSD curves obtained under growing conditions. The term K'_{attr} ($= K_{\text{attr}} \eta_{\text{removal}}$) is the product of two terms. For the case of ammonium sulfate crystals, the value of η_{removal} is unity, therefore it is lumped together with the attrition rate constant K_{attr}. Evidence for making the assumption of $\eta_{\text{removal}} = 1$ was gathered by examining the surfaces of ammonium sulfate crystals, which were sampled in the product line from the crystallizer under study in this work. The photographs showed that no loose or partially loose attrition fragments were located on the crystal surfaces, even though there was clear evidence of attrition on the crystal corners and edges (see results and discussion of photographs). Very often, these parameters are determined independently of the crystallizing system by suspending a prespecified distribution of crystals in either a saturated or inert solution. According to the models discussed earlier (Van der Heijden et al., 1994; Daudey, 1990), using this method it would only be possible to gain information about the mechanical breeding mechanism of nuclei production, as under normal crystallizing circumstances, the renewable growth structures on the crystal surfaces, would yield more attrition fragments. There is also a possibility that the distribution resulting from such experiments would be different. On top of this, little account is also taken of the properties of the suspending liquid and its possible effect on the attrition rate.

Analogous to Eq. 5, the volume rate of production of attrition fragments is given by the product of the formation and removal terms ($\dot{V}_{\text{attr}} = \eta_{\text{removal}} F$). In Eq. 5, this was calculated from first principle considerations of the mechanics of particle collisions. Here, it is suggested that from the method of moments, the production rate of attrition fragments can be calculated by Eq. 8, from knowledge of the attrition rate

function (G_{attr}) of parent crystals and the second moment of the CSD as follows:

$$\dot{V}_{attr} = \int_0^\infty G_{attr}(x)n(x)x^2dx. \tag{8}$$

The growth rate of all crystals is then expressed as the sum of the kinetic growth rate [$G_{kin}(x, \sigma)$] less the growth rate caused by particle attrition,

$$G_{eff}(x,\sigma) = G_{kin}(\sigma) - G_{attr}(x). \tag{9}$$

A constraint must also be included at this point,

$$\forall x > 0 \Rightarrow G_{eff}(x) > 0.$$

Little information exists on the form and location of the distribution assumed by the attrition fragments. For the most part, this is due to reasons of practical difficulty. The presence of a very wide distribution of sizes in a suspension crystallizer (1–2,000 μm) makes it difficult to focus in on a particular size range with conventional on-line measuring devices. The accuracy of sieving techniques is sensitive to errors introduced during the sampling and drying steps. As mentioned in the previous section, experiments carried out under a microscope have shown that by contacting a growing crystal surface with a steel rod, a log-normal distribution of particles is produced (Van der Heijden et al., 1989).

During the attrition process, stress will enter the crystal lattice (Bhat et al., 1987). Because of this, and subject to the supersaturation level in the crystallizer, some of these particles will tend to grow out while some will not, and the particles that do grow out will show a distribution in growth rates (Rusli et al., 1980). Many literature references report this phenomenon from small-scale suspended single-crystal experiments to larger scale experiments where the nuclei are produced in suspension. In the model presented here, as yet no account is taken of SDG or GRD. Implementation of a model for either GRD or SDG has been planned based on observations of the growth rate of small sub-300 μm ammonium sulfate crystals, less than 300 μm, in the crystallizer. Instead of an SDG/GRD function, an efficiency factor is defined, $\eta_{outgrowth}$, which is defined as the ratio of the volume of attrition fragments that grow out to the total volume of attrition fragments produced:

$$\eta_{outgrowth} = \frac{\text{volume of fragments that grow out}}{\text{total volume of attrition fragments produced}}. \tag{10}$$

Here, $\eta_{outgrowth}$ is assumed to be a constant factor. In reality, it will be a function of the supersaturation, as a high supersaturation will encourage crystals with a higher stress to grow out, thus,

$$\eta_{outgrowth} = k_{outgrowth}\sigma. \tag{11}$$

By using $\eta_{outgrowth}$, a certain growth rate is imposed on a fraction of the crystals, while the remaining crystals are assumed not to grow at all. Such a mechanism is more akin to fast growers/slow growers theory found in some literatur references (Garside and Larson, 1978; Daudey et al., 1990 where it was shown that particles less than 10 μm, produce by contacting a crystal surface with a steel rod, grew with very low or even zero growth rate, while crystals greater tha 10 μm grew with a growth rate that was five times greate than the crystals less than 10 μm. On the other hand, usin an SDG rate function imposes a range of growth rates on th crystals as a function of crystal size (Figure 2).

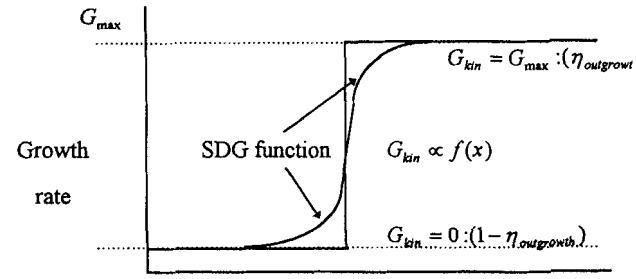

Figure 2. Growth rates based on a SDG [$f(x)$] mechanism and also on an outgrowth efficienc ($\eta_{outgrowth}$) basis.

At this point, it is now possible to derive an expression fo the rate of secondary nucleation based on the preceding con siderations. Such an expression is as follows:

$$B_{o,eff}(x) = \eta_{outgrowth}H(x)\dot{V}_{attr}. \tag{12}$$

This is subject to a condition of mass conservation

$$\int_0^\infty H(x)x^3dx = 1.$$

Assuming a log-normal distribution for the attrition frag ments, two parameters have to be specified, that is, the posi tion (x_{med}) and spread (x_s) of the distribution.

Population balance

In this form (Eq. 12), the nucleation function can be incor porated into the population balance (Randolph and Larson 1988) equation to yield the following form:

$$\frac{\partial n(x,t)}{\partial t} + \frac{\partial G_{eff}(x,t)n(x,t)}{\partial x} + \frac{Q_p n(x,t)}{V} + \frac{Q_f n(x,t)}{V}h_f(x) = B_{o,eff}(x). \tag{13}$$

Several important assumptions are made to arrive at this form.

1. The crystallizer is well mixed.
2. "Fines" are removed from an annular zone around the crystallizer. A predetermined classification function [$h_f(x)$] and a removal rate (Q_f) characterizes the fines removal sys-

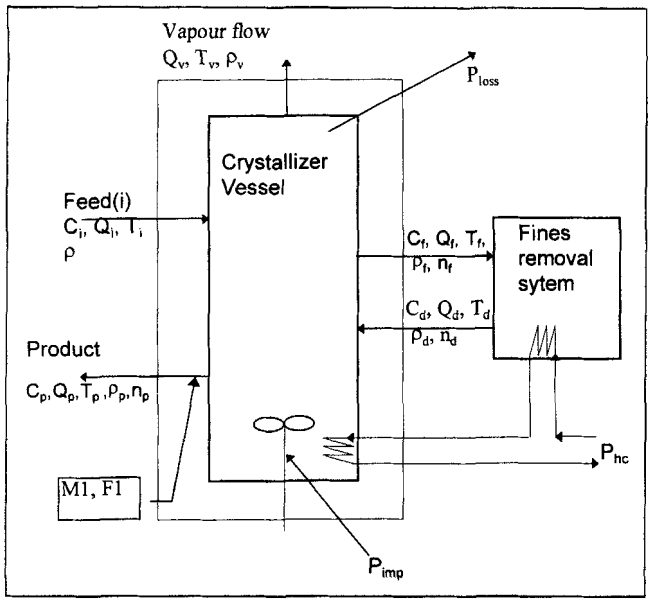

Figure 3. 970-L crystallizer.

tem (Prins, 1992). The "fine" crystals are completely dissolved in the fines dissolution system by heating the stream 10°C above the normal operating temperature, and returning the dissolved fines to the crystallizer as saturated feed at this higher temperature.

3. Crystal-free saturated feed enters the crystallizer at the same temperature as the operating temperature of the crystallizer.

4. The phenomena of growth rate dispersion and size-dependent growth do not occur.

This equation takes the form of a first-order partial differential equation (PDE) to which there is no analytical solution. Instead, it is transferred into a set of first-order ordinary differential equations using the so-called "method of lines" and solved using a second-order Runga-Kutta routine. For this purpose, the length axis is discretized into 300 classes over the range 1 to 2,000 μm.

The model is completed with a set of relations for the concentration, mass, and heat balances that are listed in the Appendix. The symbols are marked in Figure 3.

Experimental Studies

Experiments were carried out in a draft tube baffled crystallizer with a volume of 970 L. This type of crystallizer consists of an inner draft tube, around which the slurry is continuously being pumped by a variable-speed rubber-coated marine propeller operating at a constant speed of 317 rpm. Around the central zone, there is an annular zone through which small or fine crystals can be withdrawn and dissolved in an external vessel before being returned to the crystallizer as saturated feed. The model material used for crystallization was ammonium sulfate. Experiments were carried out in the evaporative mode, with the suspension held at a constant temperature of 50°C and a constant heat input to the crystallizer of 120 kW (Run 1 and 2) and 150 kW (Run 3). The crystallizer was fed with crystal-free saturated feed that was regulated to hold the suspension volume constant. The initial CSD was generated by supersaturation buildup in the crystallizer, after which a primary nucleation event took place. A representation of the plant is given in Figure 3, which shows the point at which the composition of the suspension (F1, density measurement) and the CSD (M1) is evaluated. Mass and energy balances are set up around the entire unit and also around the two subblocks (the crystallizer and fines recycle system). The system has two inputs, the crystallizer feed and the heat of evaporation (to the fines dissolution vessel and to the crystallizer itself), and two outputs, the vapor flow and the product stream containing the contents of the crystallizer. The CSD is measured on-line in the product stream with a frequency of 1 measurement/2 minutes (Boxman, 1992).

The operation of the crystallizer along with CSD measuring equipment and process monitoring and control computers, have been optimized over a number of years to enable the crystallizer to be run over long periods of time and to be able to suppress process disturbances such as line blockages quickly.

With this setup, three experiments were carried out (Runs 1, 2 and 3). After the initial primary nucleation event, the population was allowed to grow and develop over a time of 30 h (Run 1) and 15 h (Runs 2 and 3). Run 1 was carried out with fines removal being applied at a rate of 1 L/s, while Runs 2 and 3 were carried out without fines removal.

The impeller speed for Runs 1 and 2 was 317 rpm, while for Run 3, it was 370 rpm. Table 1 gives all the details regarding the operating conditions of the experiments.

Results and Discussion

Only the results of three experiments have been used for validation of the new model, which may seem like very few results on which a new model can be accurately validated, but it should be kept in mind that the results shown here result from the startup behavior of a crystallizer, directly after a nonsteady-state CSD has been produced due to a primary nucleation event. As such, the CSD first undergoes a dynamic phase in which the CSD, supersaturation, and crystal mass and total crystal surface area are continually changing, before they eventually arrive at a steady state. This, in effect, represents infinitely more data points to validate the model than the traditional approach of estimating a number of steady states achieved by varying the operating conditions over a number of experiments.

The results of Runs 1, 2 and 3 are shown in Figures 4, 5 and 6. The results are presented in terms of three characteristic sizes of the CSD (on a volumetric basis), that is, the 25% (X25), 50% (X50 or median size), and the 75% (X75) quar-

Table 1. Operating Conditions for Small-Scale 970-L Experiments

Run	Heat Input (kW)	Residence Time (min)	Fines Flow (L/s)	Temp. (°C)	Duration (h)	Impeller Speed (rpm)
1	120	75	1	50	30	317
2	120	75	0	50	15	317
3	150	75	0	50	15	370

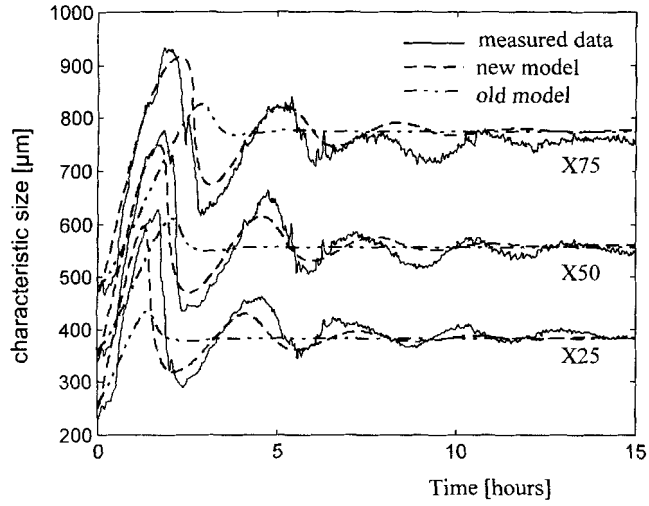

Figure 4. Run 1 (120 kW, 75 min, 1 L/s fines, 317 rpm): measured and simulated startup trends.

Note the poor performance of the power law model in predicting the dynamic behavior.

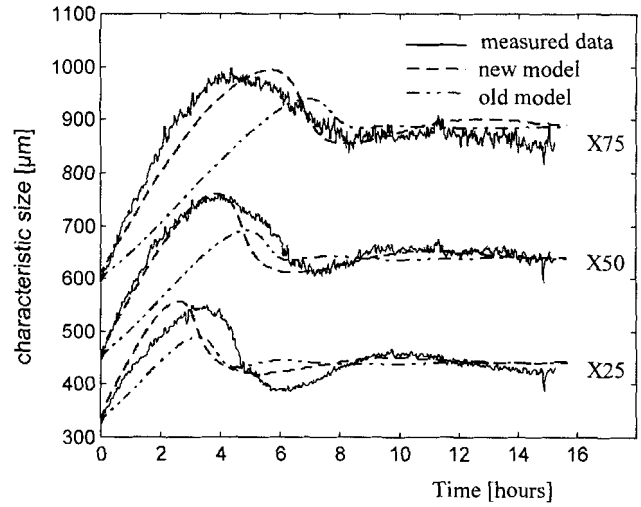

Figure 6. Run 3 (150 kW, 75 min, 0 L/s fines, 370 rpm): measured and simulated startup responses in the crystallizer.

tile. Based on the model outlined, and the mass and energy balances carried out around the crystallizer and the fines dissolution system, the entire crystallization system was simulated. Model parameters for growth, attrition, and nucleation ($\eta_{\text{outgrowth}}$) were optimized by comparing the simulated and measured CSD responses, using a quadratic convergence criterion, for the best parameter fits. The resulting optimized parameters are listed for all three experiments in Table 2. The optimized fits of the CSD, in terms of the characteristic sizes, are also shown in Figures 4, 5 and 6. Figure 7 shows the growth rates, birth rates, and the supersaturation profile, throughout all the experiments for all three runs as calculated by the simulation. In addition to showing the fit predicted by the new model proposed in this work, the response predicted by using a power-law correlation for the secondary nucleation rate is also included. The following correlation,

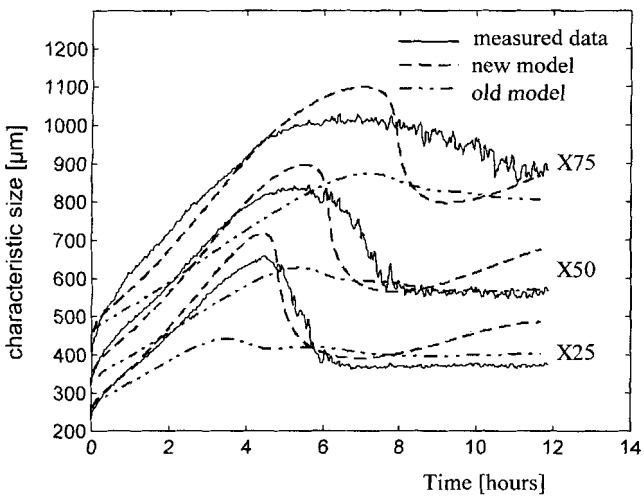

Figure 5. Run 2 (120 kW, 75 min, 0 L/s fines, 317 rpm): measured and simulated startup responses.

resulting from the experiments of other workers for the ammonium sulfate/water system in evaporative mode was used (Daudey et al., 1990; Jager, 1991):

$$B_{o,\text{eff}} \sim G_{\text{kin}}^{2.1} m_3. \tag{14}$$

The constant of proportionality was set so that the simulated nucleation rate was the same as the nucleation required to give the same median size as was measured by the Malvern for the crystallizer CSD.

By comparing the measured responses of the three experiments in terms of the characteristic sizes, it can be said that the responses of Runs 2 and 3, where no fines removal was applied, display a less oscillatory behavior than Run 1, where fines were removed at a rate of 1 L/s (previously reported by Eek et al., 1995). It was only necessary to run the crystallizer for 16 hours after the primary nucleation before the system reached an apparent steady state for Runs 2 and 3, while it took a much longer time (30 h) for Run 1 to reach a steady state. The difference in dynamic behavior between Run 1 and Runs 2 and 3 can be explained by considering what happens when fines are removed from the crystallizer. All of the crystals that are removed in the fines stream from the crystallizer are dissolved and recirculated back to the crystallizer as a supersaturated solution. This has the effect of raising the supersaturation level in the crystallizer and thus the growth rate above the value that it would have, if no fines removal was applied. This effect can be seen by examining the results of the simulation for the growth rate and supersaturation trends (Figures 7a and 7c), which indeed show that for Run 1 the supersaturation was higher throughout the entire experiment, and that it also assumes a higher steady-state value in Run 1 than in Runs 2 and 3.

One expects that the outgrowth efficiency of the attrition fragments would also be directly effected by the level of supersaturation in the crystallizer. According to the theory described previously, a higher supersaturation would allow at-

Table 2. Optimized Parameters for Runs 1, 2, and 3

Run Symbol Dimensions	Attrition			Growth		Survival	Nucleation	
	K'_{attr} m/s	x_g μm	n	K_{kin} m/s	n	$\eta_{outgrowth}$	x_{med} μm	δ
1	$2e-09$	750	13	$5e-06$	1	0.50	10	0.20
2	$2e-09$	750	10	$5e-06$	1	0.08	10	0.20
3	$2e-09$	750	10	$5e-06$	1	0.07	10	0.20

trition fragments with a higher level of internal strain to grow out. This is confirmed by the much higher outgrowth efficiency obtained for the simulation of Run 1 at an efficiency of 0.50, which means that 50% by volume of all attrition fragments produced grow out, as opposed to a 0.07 and 0.08 outgrowth efficiency for Runs 2 and 3, respectively, reflecting the lower supersaturation present in these experiments.

The large difference in outgrowth efficiencies between Run 1 and Runs 2 and 3 also yields a much higher birth rate for Run 1, as is seen in Figure 7b.

Figures 4 to 6 show that reasonably good fits can be obtained with the new model (Eq. 12) by optimizing the fit parameters to the measured CSD response. Given the accuracy of the model to predict the dynamic behavior and steady state reached by the CSD, validates the link between the volumetric attrition rate and the secondary nucleation rate proposed in this article. The results for the simulation of the CSD using the secondary nucleation correlation of Eq. 14 is also shown in Figures 4, 5 and 6. The results show that it is only possible to introduce a very small amount of dynamics into the CSD by using Eq. 14 at the start of the experiment, and that the system reaches a steady state much quicker than is observed in the measured CSD for the three experiments.

Deviations in the simulated and measured responses do exist, however, for the model proposed here, especially in Run 2. In this experiment, the measured response reaches an apparent steady state after 8 hours. At that time, the response of the simulated CSD is still oscillating. This difference could be caused by an internal classification effect where the larger particles have a longer residence time in the draft tube, thus being measured less frequently, giving a bias in the CSD measurement toward smaller sizes. This effect may then result in a lower measured median size than is actually present in the crystallizer. This effect is not seen in Run 3, as the impeller speed was higher at 370 rpm, compared to 317 rpm for Run 2. Run 1, also carried out at 317 rpm, may also be effected by internal classification, as there is a static deviation in X75 throughout the experiment between the measured and simulated responses. Unless reliable information is available on the extent of the internal classification, it cannot be taken into account in the model, as both internal classification and attrition affect the CSD in a similar way. A separate function should therefore be estimated for internal classification.

It was found that the size at which the attrition fragments were born had very little effect on the dynamic behavior or eventual steady state reached by the CSD within the range 5 to 12 μm. This range is also consistent with the observations of other workers, as discussed in the Theory section. For this reason, an arbitrary value of 10 μm was chosen for the position and a standard deviation of 0.20 was chosen for the distribution of secondary nuclei.

There is very little difference between the kinetic parameters evaluated from the three optimizations. The largest differences were in the values for the survival efficiency that were discussed earlier. The only other appreciable difference was between the value estimated for the power in the attrition correlation (Eq. 7), which is 10 for Runs 2 and 3 and 13 for Run 1. A diagram of the attrition function is given in Figure 8, using values ranging from 1 to 15. The resulting plot shows that below a size of 500 μm, the attrition rate

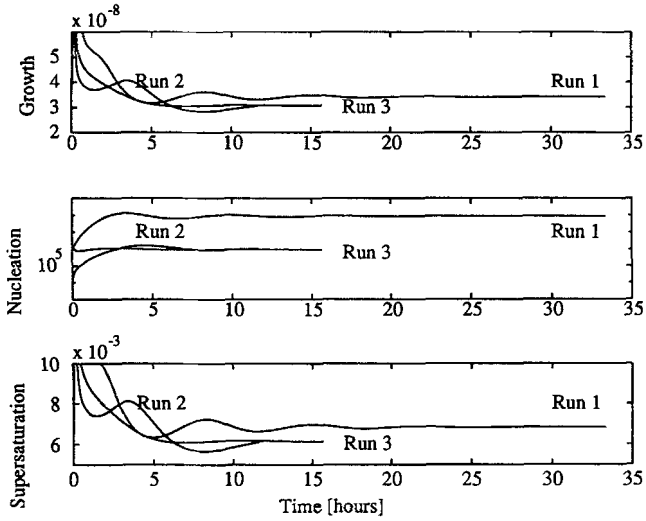

Figure 7. Simulated trends of the growth rate (top), nucleation rate (middle), and supersaturation (bottom) with time.

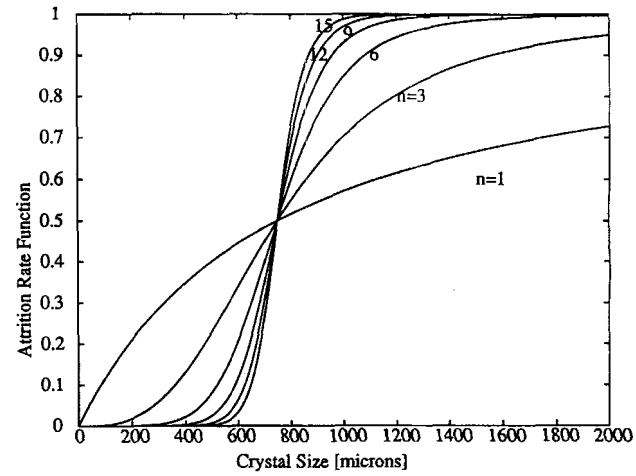

Figure 8. Form of the attrition function (Eq. 7) for various values of the exponent *n*.

Length parameter is taken as the value obtained from the simulations, that is, 750 μm.

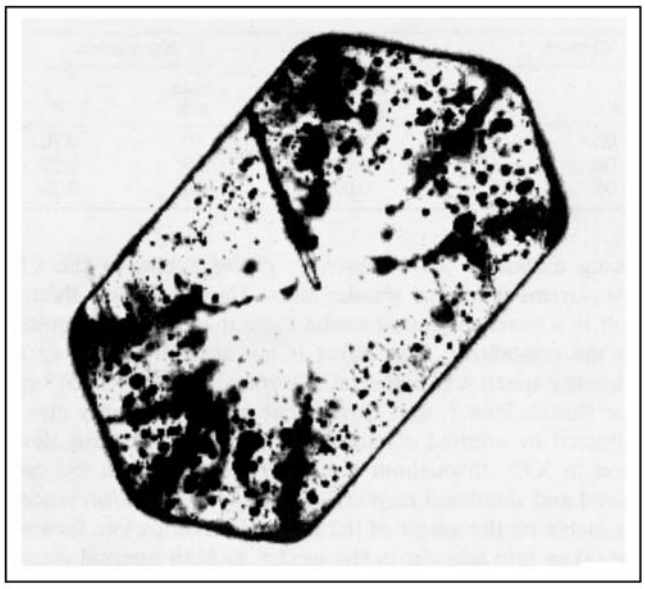

Figure 9. Optical micrograph of the internal structure of an ammonium sulfate crystal removed from the crystallizer toward the end of Run 1.
Projection is of the (110) face.

reduces to zero. Independent measurements by Jager (1990) showed that for ammonium sulphate crystals suspended in ethanol in a 20-L DTB crystallizer similar in design to the 970-L crystallizer, the onset of attrition was very sharp and began to take effect at a size of 400 μm. Further proof that attrition fragments are formed by parent crystals when they exceed a certain minimum size, was provided by examining the internal structure of ammonium sulfate crystals, removed from the product slurry of Run 1. The crystals were placed in an organic fluid having the same refractive index as ammonium sulfate. Figure 9 shows a photograph taken of a crystal internal structure using an optical microscope projected onto the (110) face. The black areas between the growth sectors are inclusions, which have formed due to the overgrowth of damaged corners and edges. In the photographs, blunt edges and corners are seen that have obviously been chipped away by an attrition process. Inside a diameter of about 500 μm in Figure 9, there are no inclusions present, which leads one to the conclusion that attrition was not prominent below this size. Figure 10 shows another crystal, but this time the photograph is taken of the (010) face. The same features can be made out, the inclusions between the growth sectors as well as other inclusions in each sector.

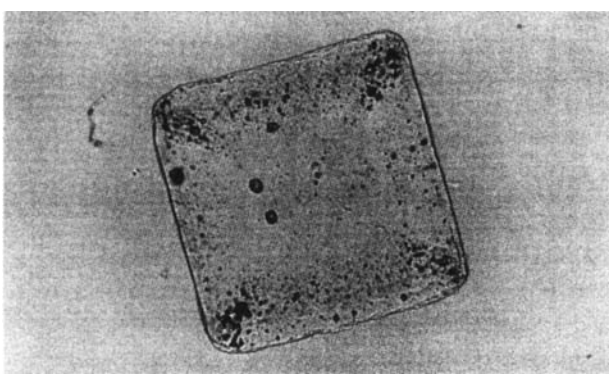

Figure 10. Optical micrograph of the internal structure of a crystal taken near the end of Run 1.
Projection shows the (101) face.

Conclusions

By coupling the secondary nucleation rate to the attrition rate, via a (survival and) outgrowth efficiency term, it is possible to obtain a good representation of the CSD dynamic behavior in a crystallizer. The new model presented here performs much better than traditional power-law correlations for the secondary nucleation rate.

Fines removal results in a higher supersaturation level in the crystallizer throughout the entire experiment, resulting in a higher survival efficiency of attrition fragments and thus a higher nucleation rate.

From the results of the parameter estimation procedures for Runs 1, 2 and 3, and from the evidence of the internal and external crystal structure, it is shown that the onset of attrition occurs quite suddenly above a certain minimum size, and can be described satisfactorily by an attrition rate function having crystal length as the only parameter.

Internal classification due to inadequate suspension of the crystal slurry may introduce a bias into the measurement of the CSD toward smaller sizes. A classification function should be estimated for the crystallizer to account for this effect in the simulation model.

Notation

$B(x)$ = length-dependent birth rate, #/m^4·s
c_p = specific heat, kJ/kg·K
C = fluid phase concentration, kg/m^3
h_p = product classification function
k' = growth rate constant, m/s
K_{attr} = attrition rate constant, m/s
K'_{attr} = attrition rate constant, m/s
$m_{attr,eff}$ = mass of attrition fragments that grow out, kg
$m_{attr,tot}$ = total mass of attrition fragments produced, kg
M_p = product density, kg/m^3
P_{hc} = heat input, kW
P_{imp} = power input via impeller, kW
P_{loss} = heat loss to the environment, kW
R_v = enthalpy of evaporation, kJ/kg
t = time, s
T = temperature, °C
V = vessel volume, m^3
x_{attr} = average size of attrition particles, m
x_g = attrition function size parameter, m
ρ = density, kg/m^3

Superscripts and subscripts

b, h, j, i, k = exponents in the power law
c = crystal
d = dissolved fines stream
f, F = fines stream
i = feed stream
p = product
v = vapor stream

Literature Cited

Bhat, H. L., J. N. Sherwood, and T. S. Shripathi, "The Influence of Stress, Strain and Fracture of Crystals on the Crystal Growth Process," *Chem. Eng. Sci.*, **42**, 609 (1987).

Botsaris, G. D., *Industrial Crystallization '75*, Plenum Press, New York (1976).
Bourne, J. R., and K. Hungerbuehler, "An Experimental Study of the Scale-up of a Well-Mixed Crystallizer," *Trans. Ind. Chem. Eng.*, **58**, 142 (1980).
Boxman, A., "Particle Size Measurement for the Control of Industrial Crystallizers," PhD Thesis, Delft Univ. of Technology, Delft, The Netherlands (1992).
Daudey, P. J., G. M. Van Rosmalen, and E. J. de Jong, "Secondary Nucleation Kinetics of Ammonium Sulphate in a CMSMPR Crystallizer," *J. Cryst. Growth*, **99**, 1076 (1990).
Eek, R. A., Sj. Dijkstra, and G. M. Van Rosmalen, "Dynamic Modeling of Suspension Crystallizers Using Experimental Data," *AIChE J.*, **41**, 1 (1995).
Garside, J., and M. A. Larson, "Direct Observation of Secondary Nuclei Production," *J. Cryst. Growth*, **43**, 694 (1978).
Garside, J., and S. J. Jancic, "Measurement and Scale-up of Secondary Nucleation Kinetics for the Potash Alum-Water System," *AIChE J.*, **25**, 948 (1979).
Grootscholten, P. A. M., B. G. M. Leer, E. J. de Jong, and C. J. Asselbergs, "Factors Affecting Secondary Nucleation Rate of Sodium Chloride in an Evaporative Crystallizer," *AIChE J.*, **28**, 728 (1982).
Jager, J., "Control of Industrial Crystallizers: The Physical Aspects," Ph.D. Thesis, Delft Univ. of Technology, Delft, The Netherlands (1990).
Jager, J., S. de Wolf, H. J. M. Kramer, and E. J. de Jong, "Estimation of Nucleation Kinetics from CSD Transients for a Continuous Crystallizer," *Chem. Eng. Sci.*, **46**(3), 807 (1991).
Landau, L. D., and E. M. Lifschitz, *Theory of Elasticity*, Pergamon Press, Oxford (1986).
Mazarotta, B., "Abrasion and Breakage Phenomena in Agitated Crystal Suspensions," *Chem. Eng. Sci.*, **47**(12), 3105 (1992).
Mersmann, A., R. Sangl, M. Kind, and J. Pohlisch, "Attrition and Secondary Nucleation in Crystallizers," *Chem. Eng. Technol.*, **11**, 80 (1988).
Nienow, A. W., and R. Conti, "Particle Abrasion at High Solids Concentration in Stirred Vessels," *Chem. Eng. Sci.*, **33**, 1077 (1978).
O'Dell, F. P., and R. W. Rousseau, "Magma Density and Dominant Size for Size Dependent Growth," *AIChE J.*, **24**, 738 (1978).
Ottens, E. P. K., A. H. Janse, and E. J. de Jong, "A Model for Secondary Nucleation in a Stirred Vessel Cooling Crystallizer," *J. Cryst. Growth*, **13/14**, 500 (1972).
Prins, B., "Fines Removal in a 970 L DTB Crystallizer," Graduate Report Thesis, Delft Univ. of Technology, Delft, The Netherlands (1992).
Randolph, A. D., and M. A. Larson, *Theory of Particulate Processes*, 2nd ed., Academic Press, New York (1988).
Rojkowski, Z. H., "Crystal Growth Rate Models and Similarity of Population Balances for Size Dependent Growth Rate and for Constant Growth Rate Dispersion," *Chem. Eng. Sci.*, **48**(8), 1475 (1993).
Rusli, I. T., M. A. Larson, and J. Garside, "Initial Growth of Secondary Nuclei Produced by Contact Nucleation," *AIChE J.*, **76**, 52 (1980).
Van der Heijden, A. E. D. M., M. Elwenspoek, and J. P. Van der Eerden, "Size Distribution of Embryos Produced by Crystal-Rod Contacts," *J. Cryst. Growth*, **98**, 398 (1989).
Van der Heijden, A. E. D. M., and Elwenspoek, M., "Contact Nuclei: In-situ and Ex-situ Observations of Surface Damaging," *J. Cryst. Growth*, **99**, 1087 (1990).
Van der Heijden, A. E. D. M., J. P. Van der Eerden, and G. M. Van Rosmalen, "The Secondary Nucleation Model: A Physical Model," *Chem. Eng. Sci.*, **49**(18), 3103 (1994).
Youngquist, G. R., and A. D. Randolph, "Secondary Nucleation in a Class II System: Ammonium Sulphate-Water," *AIChE J.*, **18**, 421 (1972).

Appendix: Model for an Evaporative Crystallizer

A well-mixed crystallizer is considered and the assumptions given in the population balance section are applied in setting up the balances for the system defined in Figure 3.

Four balances are considered: the crystal population balance, the dissolved and crystalline salt balance, the energy balance, and an overall mass balance. General equations for the system described in Figure 3 are formulated below.

Population balance

$$\frac{\partial n(x,t)V}{\partial t} = -V\frac{\partial n(x,t)G(x,t)}{\partial x} - (Q_p h_p + Q_F h_F)n(x,t) + B(x)V. \quad \text{(A1)}$$

By multiplying each term in Eq. A1 by $k_v x^3$, and by defining the voidage fraction in the crystallizer as $\epsilon = 1 - k_v m_3$, and substituting for the third moment wherever it occurs, the crystal mass balance over the crystallizer results, giving

$$\frac{\partial V}{\partial t}(1-\epsilon) - V\frac{\partial \epsilon}{\partial t} = +3k_v V\int_0^\infty Gnx^3 dx - Q_p(1-\epsilon_p) - Q_F(1-\epsilon_F) + Q_i(1-\epsilon_i) + k_v V\int_0^\infty B(x)x^3 dx \quad \text{(A2)}$$

Salt balance

$$\frac{\partial}{\partial t}[\epsilon VC + (1-\epsilon)V\rho_c] = Q_i[\epsilon_i C + (1-\epsilon_i)\rho_c] + Q_d C_d - Q_p[\epsilon_p C + (1-\epsilon_p)\rho_c] - Q_F[\epsilon_F C + (1-\epsilon_F)\rho_c] \quad \text{(A3)}$$

Energy balance

$$\frac{d}{dt}T[\epsilon V\rho c_p + (1-\epsilon)V\rho_c c_{pc}] = Q_i[\epsilon_i \rho_i c_{pi} + (1-\epsilon_i)\rho_c c_{pc}]T_i + Q_d \rho_d c_{pd} T_d + P_{\text{imp}} + P_{hc} - P_{\text{loss}} - Q_p[\epsilon_p \rho c_p + (1-\epsilon_p)\rho_c c_{pc}]T - Q_F[\epsilon_F \rho c_p + (1-\epsilon_F)\rho_c c_{pc}]T - Q_v[\rho_v R_v + \rho_v c_{pv} T]. \quad \text{(A4)}$$

Total mass balance

$$\frac{d}{dt}[V(\epsilon\rho + (1-\epsilon)\rho_c)] = Q_i[\epsilon_i \rho_i + (1-\epsilon_i)\rho_c] + Q_d \rho_d - Q_p[\epsilon\rho + (1-\epsilon)\rho_c] - Q_F[\epsilon_F \rho + (1-\epsilon_F)\rho_c] - Q_v \rho_v. \quad \text{(A5)}$$

By partial differentiation of the lefthand side of Eqs. A3, A4 and A5 and substitution with Eq. A2, the following expressions are derived for the salt energy and total mass balances.

Salt balance

$$\epsilon V\frac{dC}{dt} = Q_d C_d - Q_p C - Q_F C + Q_i C - (\rho_c - C)\left[3k_v V\int_0^\infty Gnx^2 dx\right]. \quad \text{(A6)}$$

Energy balance

$$Q_d \rho_d c_{pd} T_d + Q_i T_i \rho_i c_{pi} - Q_p \rho c_p T - Q_F T \rho c_p - Q_v[\rho_v R_v + \rho_v c_{pv} T] + P_{\text{imp}} + P_{hc} - P_{\text{loss}} - [T\rho_c c_{pc} - T\rho c_p]\left[3k_v V \int_0^\infty G n x^2 dx\right] = 0. \quad \text{(A7)}$$

Total mass balance

$$Q_d \rho_d - Q_p \rho - Q_F \rho + Q_i \rho_i - Q_v \rho_v - (\rho_c - \rho)\left[3k_v V \int_0^\infty G n x^2 dx\right] = 0. \quad \text{(A8)}$$

Equations A6, A7 and A8 form a system of three linear equations that completely define the system in terms of in- and outgoing flows and quantities. The equations must be solved to give expressions for the three unknowns, that is, the growth rate (G), the feed flow rate (Q_i), and the vapor flow rate (Q_v), assuming a Class II system ($dc/dt = 0$ and C = saturation concentration).

Derivation of the growth rate function for a Class I System

For a class I system, an extra expression can be introduced into the system of equations for the growth rate as a function of the supersaturation:

$$G = k\Delta C^n = k'\left(\frac{\Delta C}{C^*}\right)^n. \quad \text{(A9)}$$

Description of the fines removal system

$$Q_d C_d = Q_F[\epsilon_F C + (1 - \epsilon_F)\rho_c]$$
$$Q_d \rho_d = Q_F[\epsilon_F \rho + (1 - \epsilon_F)\rho_c].$$

Other definitions

$$\epsilon_i = 1 - k_v m_{3,i}$$
$$m_{j,i} = \int n_i(x) x^j dx \qquad (i = \text{fines/product/crystallizer contents})$$
$$n_p(x) = h_p n(x)$$
$$n_F(x) = h_F n(x).$$

By assuming initial conditions for the concentration in the fluid phase and a distribution of crystals present in the crystallizer after the primary nucleation step, Eqs. A6, A7, A8, A9 and the population balance A1 can be solved at regular time intervals to give the development in the CSD and concentration of ammonium sulfate in the fluid phase.

Manuscript received Dec. 27, 1994, and revision received May 30, 1995.